Appl Phys B (2009) 95: 421–428
DOI 10.1007/s00340-009-3501-4

Applied Physics B
Lasers and Optics

Photorefractive effect in $LiNbO_3$-based integrated-optical circuits at wavelengths of third telecom window

S.M. Kostritskii

Received: 24 November 2008 / Revised version: 4 March 2009 / Published online: 2 April 2009

Abstract Original results on investigation of the photorefractive effect in straight channels and integrated-optical circuits such as a directional coupler, Y-splitter and Mach–Zehnder interferometer, exploiting titanium-indiffused and proton-exchanged $LiNbO_3$ waveguides, are presented. It has been found that the photorefractive damage is non-negligible for IR radiation with wavelengths near 1.5 μm in all circuits studied. The new methods for accurate evaluation of small extents of photorefractive effect are proposed.

PACS 42.82.Bq · 42.65.Hw · 42.82.-m

1 Introduction

The photorefractive damage (PRD) is a well-known classical problem for most electro-optic and nonlinear optic applications of $LiNbO_3$ crystals: Optically induced change of refractive index creates difficulties to produce stable devices in this material for visible and near-IR ranges. This problem is most dramatic in case of integrated-optical (IO) devices, utilizing channel waveguides, due to the following specific features: (1) Light beams are confined in two dimensions to region only a few micrometers in size, and very high optical intensities are thus obtained even at small input power; (2) The inhibition of diffraction leads to effects, which do not occur in bulk samples; (3) Waveguide fabrication means heavy doping, as industrial IO $LiNbO_3$ devices are fabricated only by the two techniques: Ti-indiffusion or proton exchange.

S.M. Kostritskii (✉)
MPTE Department, Moscow Institute of Electronic Technology,
124498 Moscow, Zelenograd, Russia
e-mail: skostritskii@mail.ru

Many detailed studies were reported for straight waveguides, IO circuits and some devices operating in the visible and near-IR regions of the spectrum [1–4], but only two systematic studies were performed at 1.3 μm [5, 6] and no such study was reported yet for PRD in IO circuits at wavelengths around 1.5 μm, while some particular features were reported only for the latter wavelength range [7–9]. However, recent activities in guided-wave electro-optic and nonlinear-optic devices are directed towards optical communication applications and concentrated in the wavelength region from 1.46 to 1.63 μm, where the photorefractive effect generally decreases and, thus, it has been neglected without any experimental verification at design of all the $LiNbO_3$ integrated-optical devices for telecom and other applications. It may be regarded as the right approach for dominating part of modern devices operating at low optical intensities. However, the advanced devices are operating with the powerful IR radiation (>100 mW) [9–11]. At the same time, even a very small refractive index variation, occurring at low input power, is important to consider, if the circuit is used in a phase-sensitive system such as a fiber optical gyroscope [12]. Therefore, the IO $LiNbO_3$ circuits must be designed so that effects of the photorefractivity are adequately compensated and knowledge of photorefractive properties is required in developing advanced devices.

2 Sample fabrication techniques

A series of straight channel waveguides, directional couplers and Y-splitters, utilizing the different geometries of Y-junction branching, were delineated in optical grade X-cut $LiNbO_3$ substrates, using standard photolithographic technique. The channel width W for Y-splitters and straight waveguides was varied in the range from 4.6 to 10 μm.

The one part of substrates was proton-exchanged at 175°C for 50–70 min in pure benzoic acid; after that, substrates were annealed at 360°C for 5.85–6.5 hours. In the second part of substrates, an array of waveguide circuits was fabricated by indiffusion of an array of Ti strips. The 100-nm-thick strips were indiffused for 18–19.5 hours at the temperature of 1000°C. To suppress Li_2O outdiffusion during this process, the substrate was placed in Pt box along with $LiNO_3$ powder while dry Ar/O_2 (1.2/1) gas was circulated through the tube at 20 cm^3/min. During fast cooling-down stage after Ti-indiffusion, the dry O_2 was circulated through the tube at 30 cm^3/min.

The IO chips of a symmetrical Mach–Zehnder interferometer with 6-μm-wide arms and two Y-junctions of constant branching angle (2.6°) were fabricated by annealed proton exchange (APE) or Ti-indiffusion technique in X-cut LN substrates at conditions mentioned in the previous paragraph. The electrode structure consisted of a coplanar waveguide with three electrodes. The width of the central electrode and the inter-electrode gap were chosen to be 18 μm to arrive at a reasonable compromise between RF ohmic loss in the electrode and the impedance matching of the electrode structure to an external microwave source. Microwave bends and tapers were incorporated to provide transition from the electro-optic interaction area to the input/output ports. The total interaction length L was chosen to be 10 mm. The necessary electrode pattern was photolithographically delineated in uniform Au-Cr seed layer that was deposited over the substrate.

The preliminary study of test samples of planar waveguides gave us the possibility to determine roughly a range of fabrication parameters, where formation of a low-loss single mode channel waveguide, operating within a certain wavelength region, is expected. A target wavelength of our optimization procedure was ranged from 1520 to 1575 nm. Final optimization of the fabrication parameters was made according to data on direct measurements of the mode shape and insertion losses for each type of waveguides and IO circuits.

Most of the IO chips were fabricated by polishing their ends at a sufficient slant angle (10°) to avoid Fresnel backward reflection from air–waveguide interfaces and, hence, to escape a parasitic Fabry–Perot interferometer. However, some IO chips with straight-channel waveguides have perpendicular air–waveguide interfaces at the both optical-grade polished lateral edges.

3 Experimental results and discussion

3.1 Experiments with straight channels: modal power cut-off and phase retardation

To access the photorefractive effect at wavelengths of third telecommunication window in the various waveguides fabricated by different techniques, an effort was first made to examine optical transmission through straight channel waveguides under comparable conditions. To provide high input intensities needed for measurements, a fiber Raman laser "IRE-Polus Group, FRL-1480-600" at 1.48 μm was used. Light from the laser was coupled into the waveguides using a single-mode fiber. Waveguide outputs were measured using a 20× lens, pinhole, and infrared detector with calibrated power meter. Output power versus input power was then plotted to check for photorefractive damage. Figure 1 shows the results of photorefractive measurements performed on straight channel $LiNbO_3$ waveguides. The Ti-indiffused $LiNbO_3$ waveguides show marked degree of saturation even at the moderate input power level. The significant attenuation of output power relative to input power illustrates the high photoinduced refractive index change in the both types of $LiNbO_3$ waveguides, especially above 100 mW.

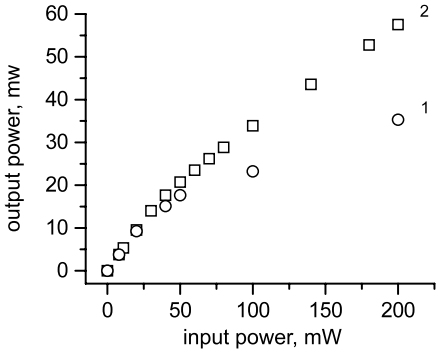

Fig. 1 Steady-state output power versus input power for the straight-channel Ti-indiffused $LiNbO_3$ (*1*) and APE:$LiNbO_3$ (*2*) waveguides. The width of waveguides is 8 μm (*1*) and 6 μm (*2*)

It has been found that the output power behavior depends dramatically on the initial mode confinement in a channel guide, i.e., confinement observed before the start of PRD. For example, a single-mode waveguide becomes more sensitive to photorefractive damage when it is closer to either fundamental-mode cut-off or double-mode regime. Thus, the measurement of output power attenuation cannot be used even for qualitative comparative study of a photorefraction magnitude in the different waveguides, as the same light-induced refractive index change may cause the different attenuation of output power, depending on initial light confinement. By the way, the qualitative studies of input power dependence of steady-state PRD and photorefractive response kinetics in a certain waveguide are possible to make, using these data. For example, the data shown in Fig. 1 allow for conclusion that steady-state PRD depends on input power and this dependence is far from saturation even at the largest input power used in both waveguides. However, these measurements are incapable of generating a quantitative measure of the steady-state photorefractive effect.

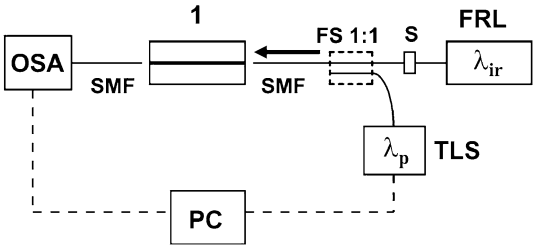

Fig. 2 Set-up for photorefractive effect measurement in waveguide FPI (*1*), consisting of a straight channel $LiNbO_3$ waveguide. *FRL*—fiber Raman laser, *TLS*—tunable laser source HP 8168 (wavelength range from 1525 to 1575 nm), *S*—switch, *FS1:1*—fiber splitter with splitting ratio 1:1, *SMF*—single-mode fiber, *OSA*—optical spectra analyzer

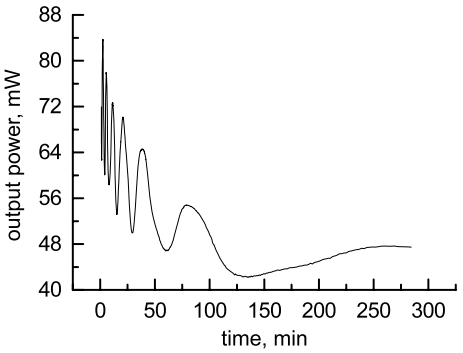

Fig. 3 Output power versus exposure time measured in FPI arrangement with 6-μm wide Ti-indiffused $LiNbO_3$ waveguide at 490-mW input power. The relatively high insertion losses (>7 dB) observed even at initial stage of this experiment are caused by an application of a photodiode (instead of OSA) with effective aperture limited by 4-mm pinhole

In order to quantify the extent of PRD, the refractive index changes were measured in the straight channel waveguides using a Fabry–Perot interferometer (FPI) arrangement. The polished end faces of the waveguide form the mirrors for the FPI. This experiment was carried out by coupling the 1.48-μm irradiation of a powerful fiber Raman laser (FRL) in a $LiNbO_3$ waveguide and monitoring output temporal power variation, Fig. 2. Note that in this experiment a closed-aperture photodiode was used to measure the output power instead of OSA, a high numerical aperture microscope objective 20× was applied, instead of output fiber, to collect the output radiation.

The change of transmitted beam power, $\Delta P(t)$, depends on the effective refractive index of a guided mode, $n^*(t)$, and wavelength, λ, as:

$$\Delta P(t) = (P_{\max} - P_{\min}) \sin^2\left\{2\pi n^*(t) L/\lambda\right\} \tag{1}$$

where $P_{\max}$ and $P_{\min}$ are the maximum and minimum output power at a certain stage of PRD, L is the waveguide length, and $(P_{\max} - P_{\min})$ depends on propagation loss [9].

The irradiation excites the electrons and leads to the charge separation and development of a temporal space charge field, $E_{sc}(t)$, that induces index change, $\Delta n^*(t)$, through the linear electro-optic effect [1]:

$$\begin{aligned}\Delta n^*(t) &= -0.5 n^3 r_{33} \times E_{sc}(t) \\ &= -\left\{(\sigma_{ph}/\sigma) E_{app} + \alpha G I/\sigma\right\} \times \left(1 - e^{-t/\tau}\right)\end{aligned} \tag{2}$$

where r_{33} is the electro-optic coefficient, G is Glass constant, α is optical absorption coefficient, $\alpha G I$ is photovoltaic current density, $\sigma_{ph} = \alpha \beta_{ph} I$ is the photoconductivity, β_{ph} is specific photoconductivity parameter, $\tau = \varepsilon_r \varepsilon_0/\sigma$ is the build-up time constant, $\sigma = \sigma_d + \sigma_{ph}$ is conductivity, σ_d is the dark conductivity, I is light intensity into guide and E_{app} is external electric field.

Both $E_{sc}(t)$ and $\Delta n^*(t)$ saturate eventually with time. The output power of transmitted beam should be modulated periodically in time, since $n^*(t) = n^*(0) + \Delta n(t)$. In fact, the recorded temporal variations of $P(t)$ were observed to start at a fast rate but slow down with time as $\Delta n^*(t)$ approaches saturation, Fig. 3. By counting the number of fringe shifts in the recorded output, the resultant maximum change in refractive index Δn^* has been estimated to be about -8×10^{-5} and -9.6×10^{-5} in APE $LiNbO_3$ and Ti:$LiNbO_3$ waveguides, respectively, at 490-mW input.

Since there is no strong absorption of the pump light used having wavelengths of around 1.48 μm, thermal effects due to absorption of the pump light are considered to be small compared to the PRD. This assumption is supported by our data on the dark decay of the light-induced effects, in which it was found that a recovery to the initial state occurs for a period of the order of ten hours. Note that the specific time of the dark decay of thermal effects is of the order of minutes [1]. It has been therefore concluded that although thermal effects may give some contribution, the observed FPI fringe shifts are due to, dominantly, PRD in the $LiNbO_3$ waveguide.

According to the theoretical and experimental findings for $LiNbO_3$ waveguide FPI [13], the significant decrease of the modulation depth $K_m = (P_{m,\max} - P_{m,\min})/(P_{m,\max} + P_{m,\min})$ with exposure, i.e. with a fringe shift number m, indicates the growth of propagation losses ε (extinction coefficient) caused by light-induced scattering due to PRD with specific kinetics (2).

The light-induced increment $\Delta\varepsilon$ of extinction coefficient may be evaluated by $\Delta\varepsilon = 4.34 \Delta K/K_0 L$, where K_0 is modulation contrast observed at initial stage of this experiment. For example, experimental data on ΔK and K_0 for waveguide FPI shown in Fig. 3 give estimation of $\Delta\varepsilon$ value of about 0.4 dB/cm, which is quite in satisfactory agreement with our data on direct measurements of insertion optical losses (increment is about 0.7 dB/cm at 490 mW) obtained in experiments similar to the one shown in Fig. 1. Such coincidence is observed in all the studied FPIs of both waveguide

types. The larger magnitude of light-induced increase of the insertion losses in comparison with the propagation losses is observed only at high input power ($\geq$100 mW) and it may be related to the light-induced increase of a mode size at the near-field output intensity profile. Such an increase of the fundamental mode width was established to be very significant at propagation of laser irradiation of the visible range in Ti:$LiNbO_3$ waveguides [14].

The application of this method at low input power is a rather difficult task as Δn^* may be not sufficient to induce even one fringe shift at a real guide length. To solve this problem, we have developed a new method for more accurate FPI experiments. Experiments were carried out by coupling two optical beams: a probe beam from a tunable laser source (TLS) to monitor the intensity transmitted through the waveguides, and an irradiation beam from FRL at 1.48 μm to induce the photorefractive damage. The polarization of each beam was oriented to excite the TE mode in the X-cut waveguides. A polarization maintaining fiber splitter (FS) was used to co-launch the two beams simultaneously. The wavelength dependence of transmission for probe beam from TLS, having the 1-pm step, was measured with aid of an optical spectrum analyzer HP 70951A. During these spectral measurements, the FRL was disconnected by switch (S) from an input port of FS and output power of the probe beam of TLS was kept below 50 μW to minimize extra damage during spectral measurements.

Our measurements before the start of photorefractive damage, i.e. before first launch of irradiation beam into waveguide, show that the spectral response of waveguide FPI presents a periodic smooth dependence of output power on wavelength of input probe beam with a fixed sequence of maxima and minima, specific for each waveguide. Impact of irradiation beam represents the shift of an interference spectrum on value $\Delta\lambda_p$, which is gradually increased by exposure via the irradiation beam, Fig. 4. This spectral dependence of output power was mathematically fitted with high accuracy, using (1). It allows to determine a small optically induced refractive index change Δn^* with very high accuracy, if a resulting phase shift at any arbitrary fixed wavelength, λ'_p, is smaller than $\pi/2$. In this case, the value of Δn^* may be evaluated from the experimental data on the gradual shift $\Delta\lambda_p$ of each interference fringe as:

$$\Delta n^*(t) = n^*(0)\left\{\Delta\lambda_p^m/\lambda_p^m(0)\right\} \tag{3}$$

where $\lambda_p^m(0)$ and $\Delta\lambda_p^m$ are positions at start of PRD and shift, because of photorefraction for certain interference fringe, m, in spectral dependence of output probe beam of damage for certain interference fringe, m, in spectral dependence of output probe beam.

Besides, the PRD induced by pump beam is accompanied by reduction of the modulation contrast K of spectral dependence, similarly to temporal dependence of output power in

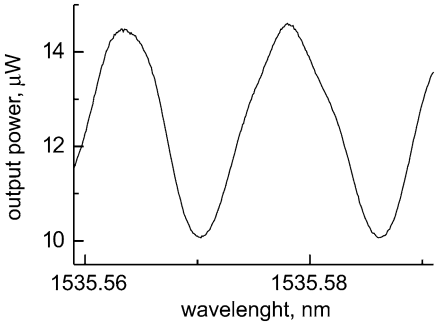

Fig. 4 Spectral dependence of output power of the weak probe beam (input power was 30 μW) for the FPI fabricated on basis of single-mode 8-μm-width straight-channel Ti-indiffused $LiNbO_3$ waveguide. FPI cavity length is 34.4 mm, channel width is 7 μm. The spectral dependence shown is obtained after extra exposure via powerful pump beam with input power of 15 mW for 3.5 hours. The latter exposure induces the decrease of wavelengths of minimum and maximum output power for each interference fringe for ~8 pm

the experiments mentioned above (see Fig. 3), and small deviation of a sequence of interference fringes from an exactly periodic law, Fig. 4. The latter may be related to the weak photorefractive intermode conversion $TE_0 \rightarrow TM_0$, according to the previous findings [1].

Note that the accuracy of measurements of both the position $\lambda_p^m(0)$ and its shift $\Delta\lambda_p^m$ is increasing with L. Therefore, to determine the changes of small photoinduced refractive index in $LiNbO_3$ waveguides, we used the relatively large samples with $L > 2$ cm and, thus, reached the high resolution in determination of $\Delta n(t)$. According to the smallest wavelength step of 1 pm possible for our tunable laser, the highest Δn resolution reached by this method is about 1.3×10^{-6}. Thus, we have determined that the steady-state value Δn_s^* (i.e., when dependence of Δn^* on t is saturated) of -10^{-5} was reached in Ti-indiffused $LiNbO_3$ and APE:$LiNbO_3$ waveguides with input power of 14 and 60 mW, respectively. This value of Δn^* was determined as critical level for performance degradation of most important IO circuits [1, 7–9].

According to the commonly used band transport model [1, 4, 11], the amount of Δn_s^* should increase with the guided power and reach a constant value at high power, depending on the ratio between photo- and dark-conductivity, and following the function $\Delta n_s^* = -[(aP)/(b + cP)]$, where P is the guided power and a, b and c are constants, e.g., $a = 9.465 \times 10^{-7}$ mW^{-1}, $b = 0.9913$ and $c = 8.984 \times 10^{-3}$ mW^{-1} in APE waveguides at excitation wavelength of 1.064 μm [11]. The saturation occurs at the value a/c, when $cP \gg b$ (i.e., at the guided power P of order of several Watts) and it is estimated to be at $\Delta n_s^* \cong -10^{-4}$. Previous experimental findings [1–8, 11] reported for wavelength range from 0.4 to 1.1 μm demonstrate that the coefficient c related to the product of specific photoconductivity and optical absorption sharply decreases with

excitation wavelength increase, while coefficient b related to the dark conductivity is, indeed, independent of wavelength. Note that dark conductivity in the both Ti-indiffused and proton-exchanged $LiNbO_3$ is much higher than in a bulk $LiNbO_3$ material [4]. Hence it might be expected that a higher power level is required to be close to saturation of $\Delta n_s^*(P)$ dependence at 1.5-μm excitation, and maximal $P = 490$ mW used by us is significantly smaller than this level.

3.2 Directional couplers

The comparative study of the different 1.5-μm-band integrated-optical $LiNbO_3$ circuits has showed that the directional couplers are most sensitive to the photoinduced damage effects. This finding coincides with all the previous comparative studies performed at the different wavelengths of visible and near-IR ranges [1, 8, 9].

A passive directional coupler shown in Fig. 5 is designed so that each arm of the coupler is a single mode at the wavelength of interest, in this case ~1.5 μm. Thus, the coupler supports the symmetric and antisymmetric supermodes, which have different propagation constants β_0 and β_1, respectively. These passive couplers were observed to undergo asynchronous, oscillatory power exchange, deviating from its stable baseline signal at high input power. It has been established that a fraction of the total energy oscillates between the throughput P_1 and crossover P_2 channels, but it is never totally transferred to the crossover channel. Amplitude of this oscillation is gradually damped with time and some steady-state stage is reached finally with an arbitrary value of the ratio P_1/P_2. Kinetics of the latter saturation process is well described by the build-up time of photorefractive effect (see (2)). Thus, it may be concluded, that effective or critical coupling length l_c' of the directional coupler is increased due to photorefraction, as from coupled-mode theory [15, 16], the output power ratio of this coupler being expressed as

$$P_2/P_1 = \tan^2(\pi L/2l_c') = \tan^2(\Delta\beta' L/2 + \theta_r) = \tan^2\left(\pi L/2l_c + 2\pi L\Delta n^*(t)/\lambda + \theta_{rc}\right) \quad (4)$$

where θ_{rc} represents the amount of residual coupling which occurs over the tapered region after the interaction length L,

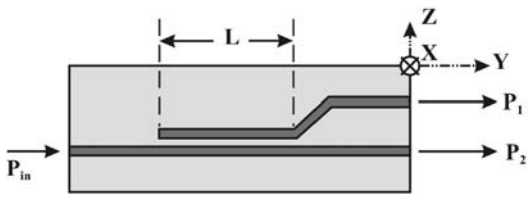

Fig. 5 Illustration of a passive directional coupler including 7-μm channels with 7-μm gap and interaction length L. P_{in}—input power, P_1 and P_2—output throughput and crossover powers

$\Delta\beta' = \Delta\beta + \Delta\phi_r$ is the difference between propagation constants in photorefractive waveguide, $\Delta\phi_r$ is relative phase retardation caused by photorefractive effect, $\Delta\beta = \beta_0 - \beta_1$, and $l_c = \pi/\Delta\beta$ is the critical coupling length needed to couple all of the power from one guide to the other in the absence of photorefractive effect, i.e., at $\Delta n^*(t) \approx 0$.

A critical parameter of active directional coupler, i.e. electro-optically controlled amplitude modulator (switch), is the crosstalk of the switching in the crossed state, when all of the light coupled into the second guide (P_2 has the maximally possible value, and $P_1 \to 0$, Fig. 5). When noted in decibels (dB), the crosstalk is:

$$\mathrm{CT} = 10 \times \lg\left[P_1/(P_1 + P_2)\right] \quad (5)$$

where P_1 and P_2 are the output powers of the initial guide and the coupled guide.

The significant effect of the photoinduced index change upon crosstalk of a Ti:$LiNbO_3$ directional coupler was observed previously [1, 5, 6] in the wide wavelength range from 0.633 to 1.3 μm. Thus, to achieve a crosstalk level of −30 dB at 1.3 μm in the 8-mm-long (7-μm-gap) active Ti-indiffused directional coupler, the light intensity should be kept below 5×10^2 W/cm^2 and −20 dB level is observed at about 2×10^3 W/cm^2, which corresponds to extremely low input power of ≤150 and ≤600 μW, respectively [6]. Our experimental data show that the active directional couplers, operating at wavelengths near 1.5 μm, have a higher threshold of the photorefractive damage: a steady-state crosstalk level of −20 dB is achieved at input power of about 10 and 35 mW in Ti-indiffused and APE $LiNbO_3$ couplers, respectively.

3.3 Y-junction branching and Y-splitters

Optical waveguides in lithium niobate are a very useful technique for building a variety of IO components. For example, the key component of fiber optical gyroscope (FOG) is the multifunction integrated optics chip (MIOC), which is an important part of the Sagnac interferometer [12]. As the MIOC consists inherently an Y-junction branching, the photorefractive effect can present the more dramatic problem, comparing to straight channel, if a change of refractive index is sufficient to induce even a small variation in the mode coupling between two channel waveguides, representing the arms of Y-junction near splitting point that can be regarded as a directional coupler with short coupling length [15].

To fabricate a low-loss Y-splitter, we utilize a Y-junction (section II) formed by three single-mode channel waveguides with width $W = 6$ μm (sections I and III), Fig. 6. The Y-junction topology is described by the following equation:

$$y(x) = y_s + \frac{y_e - y_s}{x_e - x_s}(x - x_s) \quad (6)$$

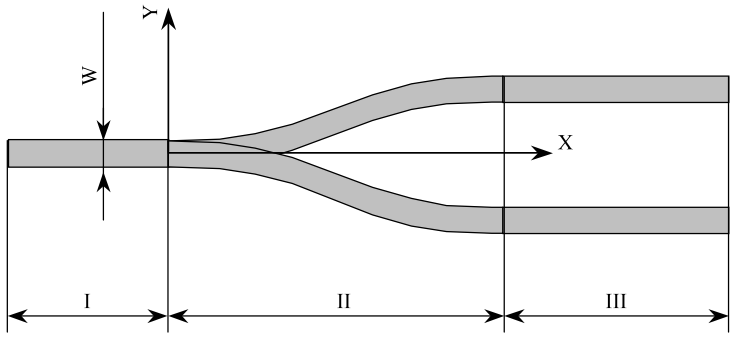

Fig. 6 Schematic illustration of Y-junction splitter utilizing a Y-junction (section II) formed by three single-mode channel waveguides (sections I and III) with channel width W

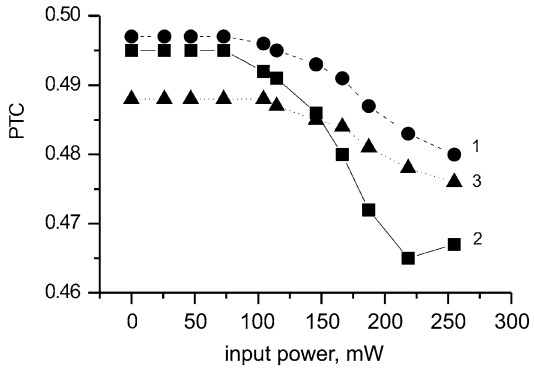

Fig. 7 Dependence of the steady-state value of power transfer coefficient (PTC) on input power P_{in} for Y-junction power dividers (branching angle $\theta = 1.9°$, $W = 6$ μm, see Fig. 6), utilizing the different types of channel $LiNbO_3$ waveguides: *1*—proton-exchanged with $PTC_0 = 0.497$; *2*—Ti-indiffused with $PTC_0 = 0.495$; *3*—proton-exchanged with $PTC_0 = 0.488$. Variation of PTC_0 values is caused mainly by imperfections of photolithography process, e.g., the dividers #1 and 3 were fabricated at the same technological conditions. PTC_0 is evaluated as a ratio between smaller output power and the sum of both output powers measured at input power ≤2 mW

where x_e and y_e have values of 11 and 0.16 mm, respectively. The width of tapered subsection of Y-junction's section II is 2W near the splitting point, having coordinates x_s and y_s. Section II presents the analog of the directional coupler with weighted coupling.

The power transfer coefficient (PTC) is established to be critical parameter PTC of the Y-junction branching, as this parameter is most sensitive to PRD influence. PTC is evaluated experimentally as a ratio between smaller output power and the sum of both output powers, i.e. PTC is directly related to a splitting ratio, which is the main parameter characterizing performance of the power divider. For example, the marked attenuation of PTC, i.e. significant degradation of power dividers' performance, is observed in all the 1.5-μm-band Y-branching power dividers even at moderate input power (50–250 mW), Fig. 7. This effect is observed at the first time, i.e. when the new consequence of PRD is discovered.

A perfect Y-junction power divider should have PTC = 0.5, and deviation of initial PTC (PTC_0 observed at $t \to 0$, or at any t with a low input power ranged from 30 to 100 μW) from this value is caused by parasitic asymmetry of Y-branching section due to technological imperfections and modes of interaction, as this branching section may be regarded as analog of the directional coupler with weighted coupling [15]; i.e. a normalized deviation parameter (0.5-PTC) is proportional to $\Delta\beta/\theta\gamma_3$, where $\Delta\beta$ is accidental asymmetry of Y-junction caused by technological imperfections, Θ is branching angle, γ_3 is transverse component of phase constant. Hence, our experimental data allow for assumption that γ_3 is altered by photorefractive effect.

In general, the following statement may be derived from experiments with the Y-branching power dividers based on Ti-indiffused and APE $LiNbO_3$ waveguides: a smaller value of PTC_0 is a higher susceptibility to PRD, i.e. $|\partial(\mathrm{PTC})/\partial P_{in}|$ is larger at the moderate input power. Experimental study of different power dividers with similar PTC_0 shows that $|\partial(\mathrm{PTC})/\partial P_{in}|$ is larger at application of Ti-indiffused $LiNbO_3$ waveguides in comparison with the proton-exchanged ones. The attenuation of PTC has power-dependent kinetics specific for PRD (2) that is the most dangerous feature of a photorefractive power divider at application in phase-sensitive systems. Therefore, even a very small temporal variation of PTC ($\geq 10^{-3}$), occurring at low input power, may present dramatic problem for some particular applications.

Thus, consideration of the photorefractive effect at a careful design of the Y-junction branching is mandatory to obtain the high performance MIOC. According to the theory of Y-junction [15, 16], to minimize a light-induced change of PTC, the branching angle θ may be increased, but a branching loss (α_b) will grow. Thus, $\theta = 1.9°$ is evaluated as an optimal value for the low input power (≤10 mW), when $\alpha_b = 0.6$ dB. The value of branching angle θ near 3.4° is theoretically determined as more suitable for high-power application, as Y-splitter should be more stable relative to influence of photorefractivity, i.e. PTC is expected to be practically constant at input power of ≤120 mW, but

$\alpha_b = 1.3$ dB. Further increase of θ is out of practical interest, as it will induce sharp growth of α_b.

According to the theory of closed-loop FOG [12], the ratio $\Delta PTC/PTC_0$ for light-induced change of Y-splitter performance should be ≤ 0.02 at application of MIOC in a high-precision FOG (bias drift $\leq 0.01°$/h). It means that output power of superluminescent diode, which is used as a light source with the center wavelength of 1.52–1.56 μm, should be limited by 13 and 55 mW in Ti-indiffused and proton-exchanged MIOCs, respectively.

3.4 Mach–Zehnder interferometers and interferometric modulators

Since IO Mach–Zehnder (MZ) interferometer is symmetric two-arms circuit, it should be most stable against small and moderate extent of photorefractive damage, which was confirmed experimentally at 1.3 [7, 8] and 1.48 μm [9]. However, some undesirable consequence of photorefractive effect (e.g., DC drift [8, 9]) becomes evident only at application of MZ interferometers in electro-optical intensity modulators. Therefore, our investigation was focused on the input-power dependence of switching capability of the (MZ) interferometeric modulators fabricated in X-cut $LiNbO_3$.

To characterize the switching capability, we measure the modulation extinction ratio (MER) at the steady state, i.e. after long-term (order of few or tens hours) illumination:

$$\mathrm{MER} = 10 \times \lg(P_{\max}/P_{\min}) \tag{7}$$

where $P_{\max}$ and $P_{\min}$ are maximum and minimum values of output power observed at variation of external DC-voltage applied on modulator electrodes.

To measure $P_{\max}$ and $P_{\min}$, the DC-voltage was gradually varied within the range from -34 to $+34$ V, inducing a $\cos^2$-like dependence of output optical power on applied voltage. This dependence has three maximums and two minimums for the output power.

Our experimental study shows that MER depends on the input power P_{in} at moderate and high power levels in all our MZ interferometric modulators. However, quantitative character of this dependence is very different even for MZ modulators fabricated at the same technological conditions. Such a particularity has been attributed to the inherent asymmetry of Y-junction regions, appearing due to technological uncertainty of photolithography and etching processes. In general, the following statement may be derived from experiments with various modulators: a smaller value of initial MER (observed at $t \to 0$, or at any t with a low input power ranging from 50 to 100 μW) is a higher susceptibility to photorefractive damage. This statement is valid in comparison of the same type (proton-exchanged or Ti-indiffused) $LiNbO_3$ modulators with quite large initial MER values of ≥ 25 dB. The most dramatic photoinduced change of MER was observed in MZ interferometric Ti-indiffused $LiNbO_3$ modulator with the initial MER = 25 dB, as steady-state value of MER observed at $P_{\mathrm{in}} = 120$ mW was 19 dB.

To develop theoretical explanation of input-power dependent MER, we consider that as Mach–Zehnder interferometer consists of two Y-junction splitters, MER should depend on PTC of Y-junction splitters and asymmetry of interferometer arms δ [16, 17]:

$$P_{\max}/P_{\min} = \left\{1 + \Delta\delta + \left[\left(1-\delta^2\right)\left(1-\Delta^2\right)\right]^{1/2}\right\}/(\Delta+\delta)^2 \tag{8}$$

where $\Delta = (1 - 2 \times \mathrm{PTC})$. Note that we assume that both Y-junction splitters have the same PTC value.

Thus, our model explains the light-induced degradation of MER as consequence of PTC change (see Fig. 7) caused by photorefractive effect in Y-junction splitters consisting of MZ interferometer. Moreover, there is a rather good quantitative correlation between theoretical and experimental data. For example, (7), (8) give MER = 29 dB at $\delta = 0.06$ and PTC = 0.495, while MER = 19 dB is obtained at PTC = 0.465 and $\delta = 0.06$. Such a variation of PTC is in good accordance with data on light-induced changes of PTC for Y-junction splitters, Fig. 7.

4 Conclusion

The photorefractive effect is found to be non-negligible in the integrated-optical $LiNbO_3$ circuits intended for practical applications at wavelengths of third telecommunication window. The directional couplers, Y-branching power dividers and MZ interferometers exhibit the light-induced degradation of important parameters even at a moderate input power, where light-induced cut-off of guided light is not observed. Besides, the influence of photorefractive effect on splitting ratio of Y-junction and modulation contrast of MZ interferometric modulators have been observed at the first time.

References

1. V.E. Wood, P.J. Cressman, R.L. Holman, C.M. Veber, Photorefractive waveguides, in *Topics Appl. Phys.*, vol. 61, ed. by P. Gunter, J.-P. Huignard (Springer, Berlin, 1989), pp. 45–100
2. R.A. Becker, R.C. Williamson, Appl. Phys. Lett. **47**, 1024 (1985)
3. R.A. Becker, Proc. SPIE **578**, 12 (1985)
4. T. Fujiwara, R. Srivastava, X. Cao, R.V. Ramaswamy, Opt. Lett. **18**, 346 (1993)
5. G.T. Harvey, G. Astfalk, A.Y. Feldblum, B. Kassahuh, J. Quantum Electron. **22**, 939 (1986)
6. G.T. Harvey, J. Lightwave Technol. **6**, 872 (1988)
7. Y. Fujii, Y. Otsuka, A. Ikeda, IEICE Trans. Electron. **E90-C**, 1081 (2007)

8. D.B. Maring, S.M. Kostritskii, R.F. Tavlykaev, R.V. Ramaswamy, Integrated Photonics Research, OSA Technical digest, RTuK4-1, 281 (1999)
9. S.M. Kostritskii, in *Technical Digest of the Workshop Lithium Niobate from Material to Device, from Device to System*, Metz, France, May 23–25, 2005, pp. 59–64 (2005)
10. N.A. Riza (ed.), *Photonic Control Systems for Phased Array Antennas*. SPIE Milestone Series, MS 136 (1997)
11. J.-P. Ruske, B. Zeitner, A. Tunnermann, A.S. Rasch, Electron. Lett. **39**, 1048 (2003)
12. H. Lefevre, *The Fiber–Optic Gyroscope* (Artech House, Norwood, 1993)
13. R. Renger, W. Sohler, Appl. Phys. B **36**, 143 (1985)
14. J.C. Chon, W. Feng, A.R. Mickelson, Appl. Opt. **32**, 7572–7590 (1993)
15. H. Saaki, I. Anderson, IEEE J. Quantum Electron. **QE-1**, 883 (1978)
16. W.K. Burns, A.F. Milton, Waveguide transitions and junctions, in *Guided-Wave Optoelectronics*, ed. by T. Tamir (Springer, Berlin, 1988), pp. 89–144
17. H. Nishihara, M. Haruna, T. Suhara, *Optical Integrated Circuits* (McGraw-Hill, New York, 1985), pp. 36–44